J Mater Sci: Mater Electron (2016) 27:2800–2808
DOI 10.1007/s10854-015-4093-x

CrossMark

Effects of substrate temperature on the properties of sputtered TiN thin films

Nader Ghobadi[1] · Mohsen Ganji[1] · Carlos Luna[2] · Ali Arman[3] · Azin Ahmadpourian[4]

Received: 24 August 2015 / Accepted: 15 November 2015 / Published online: 23 November 2015
© Springer Science+Business Media New York 2015

Abstract In the present work, high quality nanostructured thin films of titanium nitride with nanoscale grain sizes have been prepared by the reactive magnetron sputtering method examining the effects of the substrate temperature on the topography, optical and semiconductor properties of the thin films Concretely, the three dimension surface topography of samples was investigated by atomic force microscopy determining the power spectral density functions. Also, a new revised version of the Tauc's method (named ineffective thickness method) has been proposed for the determination of the optical band gap in nanostructure semiconductor thin films. These studies indicated that the increment of the substrate temperature improves the physical properties of the films modifying the grain size and grain aggregation, and altering the optical band gap of the samples from 4.06 to 3.43 eV. In addition, a competitive growth of crystalline planes with different orientations was found as a result of the occurrence of higher grain sizes in the nanostructured titanium nitride thin films.

✉ Nader Ghobadi
n.ghobadi@malayeru.ac.ir

1 Physics Department, Faculty of Science, Malayer University, Malayer, Iran

2 Facultad de Ciencias Físico Matemáticas, Universidad Autónoma de Nuevo León, Av. Pedro de Alba s/n, San Nicolás de los Garza, 66455 Nuevo León, Mexico

3 Young Researchers and Elite Club, Kermanshah Branch, Islamic Azad University, Kermanshah, Iran

4 Departments of Physics, Kermanshah Branch, Islamic Azad University, Kermanshah, Iran

1 Introduction

Titanium nitride (TiN) materials with suitable band-gap energies have been extensively applied for optical transmittance applications in the visible region [1], and recently TiN films have attracted much attention in the fields of energy-saving due to their astonishing properties [2]. Concretely, TiN thin films are low cost and easy-to-prepare materials that exhibit free-electron-like behaviors, good electrical conductivity values, and optical properties suitable for solar control coatings and transparent electrodes [3]. Also, titanium nitride is frequently used as a surface coating on cutting tools due to its excellent mechanical properties [4–8], and the chemical inertness of TiN makes itself a valuable corrosion protective coating [8]. The combination of these properties allows further considerations of TiN films, being an exceptional system for its use as the counter electrode of dye-sensitized solar cells [3]. In addition, the properties of the TiN thin films can be finely tailored with the controlled variation of the synthesis conditions. For instance, the preparation of titanium nitride thin films by sputtering techniques at sufficiently high temperatures leads to compositions close to that of stoichiometric bulk matter [3], moreover, the substrate temperature may have a considerable effect on some properties of the TiN thin films such as its crystalline orientation. On the other hand, the deposition rate and grain size of TiN thin films decrease as the ratio of nitrogen to argon in plasma atmosphere is increased [4]. This fine modulation of the TiN thin films properties is currently exploited to explore quantum confinement effects of low dimensional semiconductor materials, exhibiting size-dependent electronic band gap energies. Moreover, the study of the surface effects of these nanoscale systems arising from their high surface to

volume ratio is crucial for the understanding of the complex nano-tribology phenomena and the surface physics, underscoring the physical, chemical and thermodynamic mechanisms involved in their fabrication [9–11]. Thus, it is essential for these topics of research to have suitable methodologies for the analysis and characterization of mechanisms and properties at the nanoscale level. In this regard, determining the three dimensional (3-D) surface topography is crucial to confirm the quality and features of thin films. It is known that engineering surfaces are often random, isotropic or anisotropic, and either Gaussian or non-Gaussian. On the other hand, although root mean square (RMS) roughness parameter provides information about the 3-D surface topography, it doesn't make any difference between peaks and valleys. Therefore, power spectral density (PSD) function is more suitable to explain the optical multilayer coating. In this framework, statistical and fractal descriptions have been mainly used for the characterization of the 3D engineering surface [12–15].

In the present work, the effects of the substrate temperature on the growth and physical properties of nanostructured TiN thin films deposited by reactive magnetron sputtering methods have been investigated by atomic force microscopy (AFM), determining the power spectral density (PSD) functions. Also, a new revised version of the Tauc's method (named ineffective thickness method, ITM) has been proposed for the determination of the optical band gap in nanostructure semiconductor thin films.

2 Experimental procedures

2.1 Preparation of samples

The sputtering system used to prepare TiN thin films is composed of the following elements:

1. A vacuum chamber with a diameter of 600 mm and a height of 500 mm.
2. A substrate holder mechanism capable to hold six substrates simultaneously and that allows users to rotate them.
3. A fully automated vacuum system including a rotary and a turbo molecular pump, a barometer and two gas valves. This vacuum system can lessen the vacuum chamber pressure to 10^{-5} mbar.
4. A quartz oscillator to determine and monitor the thickness of the films during the deposition process.
5. Two plane magnetrons placed beneath two target holders, one of them is utilized for DC magnetron sputtering, while the other one is used for RF magnetron sputtering.
6. Two mass flux controllers to control the amount of sputtering and reactive gases (Ar and N_2 respectively) in sccm (standard cubic centimeters per minute).
7. A substrate heater to control and monitor the deposition temperature.
8. A 600 W RF power supply and a 1500 W DC power supply.

A titanium disk of very high purity (more than 99 %) and six glass substrates were used in the preparation of samples. The substrates were washed in trichloroethylene, acetone, alcohol and distilled water respectively under ultrasonication. The target (titanium disk) was set on a plane magnetron in the vacuum chamber and the target holder had a negative bias voltage (i.e. the target was on the cathode) whereas the vacuum chamber and substrate holders were in the anode of the system. In addition, the substrates were cleaned by ion bombardment in an argon flow of 40 sccm discharge for 10 min. After wards, a very thin titanium layer was deposited on the substrate using Ar only for 10 min, which is favorable for increasing the adhesion of the main film and reduces the residual stress between TiN and substrate surfaces [16].

In this study six thin titanium nitride films (named from S-1 to S-6) were deposited on glass substrates having different temperatures from room temperature to 400 °C. The other experimental parameters were fixed as shown in Table 1.

2.2 Characterization of the TiN thin films by X-ray diffraction (XRD)

X-ray diffraction (XRD) patterns of samples were measured at room temperature using a diffractometer with Cu Ka ($\lambda = 1.54060$ Å) radiation. The crystal sizes of the films were calculated using the XRD results by means of Scherrer equation [17]:

Table 1 Constant experimental parameters for preparing TiN thin films

ArFlow rate (sccm)	N_2 flow rate (sccm)	Base pressure (mbar)	Working pressure (mbar)	Deposition time (h)	Ionic current (A)	Voltage (V)	Power (W)
40	2	4.5×10^{-5}	2×10^{-3}	2	0.95	370	350

$$L_{(hkl)} = \frac{0.9\,\lambda}{\beta \cos\theta} \quad (1)$$

where λ is the X-ray wavelength, β is the broadening of the diffraction peak (after subtracting the instrumental broadening), and θ is the diffraction angle at which the peak maximum occurs.

2.3 Characterization of the TiN thin films by atomic force microscopy (AFM)

The characterization of the topography of the six samples was carried out by AFM in non contact mode using a Nanoscope Multimode atomic force microscope (Digital Instruments, Santa Barbara, CA), using scan rates of 10–20 µm/s to obtain 256 × 256 pixel images. These characterizations were carried out at room temperature using cantilevers with the nominal properties for force-distance curve measurements. All images were obtained over square areas of 4.4 µm × 4.4 µm.

2.4 Characterization of the TiN nanostructured thin films by power spectral density (PSD) function

The power spectral density function of the bidirectional reflectance distribution function (BRDF) was determined from the AFM surface profile data. In this work, the PSD function was determined using the following equation [18, 19]:

$$S_2(f_x,f_y) = \frac{1}{L^2}\left[\sum_{m=1}^{N}\sum_{n=1}^{N} Z_{mn} e^{-ei\pi \Delta L(f_x m + f_y n)} (\Delta L)^2\right]^2 \quad (2)$$

where S_2 denotes the two-dimensional PSD, L is the scanned surface area, N is the number of data points per line and row, Z_{mn} is the profile height at position (m, n), f_x, f_y are the spatial frequency in the x- and y-directions and $\Delta L = \frac{L}{N}$ is the sampling distance.

2.5 Characterization of the samples by UV–visible spectroscopy

The ultraviolet–visible (UV–visible) spectra of the nanostructured thin films were recorded using a UV–vis spectrometer (Perkin-Elmer, UV/VIS Spectrometer Lambda25-USA) in a wavelength range of 190–1100 nm.

3 Ineffective thickness model (revisited Tauc's model)

Firstly, we prove that the energy band gap is independent on the thickness measurement. In semiconductors, the following equation has been obtained to relate the absorption coefficient to incident photon energy [20]:

$$\alpha(v)hv = C(hv - E_{gap})^m \quad (3)$$

where E_{gap}, C and hv are the optical energy gap, a constant and the incident photon energy, respectively; $\alpha(v)$ is the absorption coefficient defined by the Beer-Lambert's law as $\alpha(v) = \frac{2.303\times A(\lambda)}{d}$, where d and $A(\lambda)$ are the film thickness and film absorbance, respectively, and m is an index that can have different values: 1/2, 3/2, 2, 3. Equation (3) can be rewritten as follows:

$$(\alpha(v)hv)^{1/m} = C(hv - E_{gap}) \quad (4)$$

By means of the Beer-Lambert's law, it is possible to rewrite Eq. (4) as:

$$\left(\frac{2.303\times A(\lambda)}{d}hv\right)^{1/m} = c(hv - E_{gap}) \quad (5)$$

and Eq. (5) can be rewritten as:

$$\left(\frac{2.303}{d}\right)^{1/m}(A(\lambda)hv)^{1/m} = c(hv - E_{gap}) \quad (6)$$

where $\left(\frac{2.303}{d}\right)^{1/m}$ is a constant, so:

$$(A(\lambda)hv)^{1/m} = \frac{C}{\left(\frac{2.303}{d}\right)^{1/m}}(hv - E_{gap}) \quad (7)$$

$\frac{C}{\left(\frac{2.303}{d}\right)^{1/m}}$ is another constant, so we can rewrite Eq. (7) as follows:

$$(A(\lambda)hv)^{1/m} = K(hv - E_{gap}) \quad (8)$$

where K is a constant and Eq. (8) can be used in a new method to determine the optical band gap upon absorbance spectra instead of absorption coefficient, avoiding any needs to determine the film thickness.

Optical absorption is the most commonly used technique in exploring the quantum effects in nanostructure semiconductor. By using this method, one can show the development of discrete features in the spectra and the enlargement of the energy band gap in nanostructured semiconductors.

4 Results and discussions

Figure 1 shows the XRD patterns of the six samples. These patterns indicate that the diffraction of (222) crystalline planes is negligible when the substrate temperature is the room temperature, however this contribution increases as the substrate temperature rises up to 250 °C. The intensity of XRD peaks corresponding to (111) preferred orientation also increases when the temperature rises up to this value

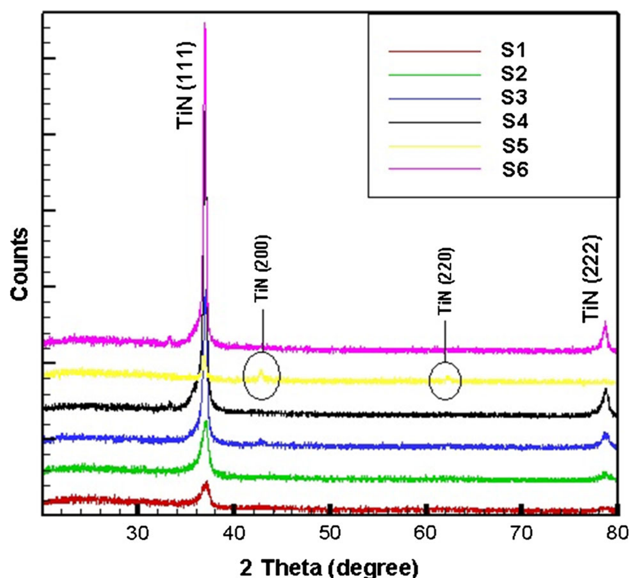

Fig. 1 XRD patterns of the prepared thin films: (a) S1, (b) S2, (c) S3, (d) S4, (e) S5 and (f) S6

(250 °C), as shown in Fig. 1. At 300 °C the (222) diffraction peak disappears, and small (200) and (220) peaks are observed, showing changes in the crystalline orientations. The intensity of XRD peaks also decrease and are wider at this substrate temperature, which leads to a slight decrease in grain size. Increasing the temperature up to 400 °C diminishes the (200) and (220) orientations and also increases the diffraction peak intensities ascribed to the (111) and (222) crystalline planes, as shown in Fig. 1. It means that the films growing at this temperature have very suitable crystalline order with relatively bigger grain sizes and better physical properties.

Figure 2 shows the crystal size calculated by means of Eq. (1) and the data of the (111) diffraction peak as a function of the substrate temperature. This dependence indicates that increasing the substrate temperature, generally leads to increased crystal sizes in the [111] direction due to the improving of the crystalline order of

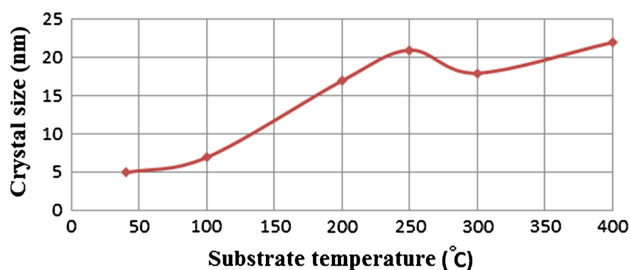

Fig. 2 Crystal size in the [111] direction of the prepared films, estimated using the Scherrer equation, versus the deposition temperature

the films. There is a negligible decrease in the grain size of the film S-5 that is due to the competitive growth of the film in other crystalline orientations as shown in Fig. 1e.

Representative 2-D and 3-D AFM images for scanning areas of 4.4 µm × 4.4 µm of the six samples are presented in Fig. 3. Also, the corresponding distributions of the peak heights observed in the AFM images are shown in the same figure, where the vertical axis represents the number of peaks per area unit. According to these histograms, the average particle size in the direction perpendicular to the film surface are around 14, 10, 15, 23, 12 and 13 nm for samples S_i with i = 1 to 6, respectively. The fluctuations of these mean particle sizes with the increment of the substrate temperature are probably due to the above-mentioned fluctuations of the thin film deposition rate and the occurrence of secondary particle growths by aggregation and coalescence [21]. The difference between the crystal size along the [111] direction (Fig. 2) and the average grain size in the direction perpendicular to the film surface (Fig. 3) probably is due to the stacking of the grains that yield to the convolution of the actual grain size with the size of the AFM tip.

Table 3 shows the characteristic parameters that describe the surface characterization of the AFM images (according with ISO 25178-2: 2012) for the six samples. These parameters are described in the “Appendix”. The S_a and S_q parameters are strongly correlated to each other but the S_q parameter has more statistical importance that S_q, is a dispersion parameter defined as the root mean square value of the surface within the sampling area and is a very general and widely used parameter.

It is observed that both parameters increase as the substrate temperature increases up to 250 °C, however, a sudden fall is observed at 250 °C, followed by a slight increase. Also, the skewness exhibits a similar tendency. These dependencies are correlated with the variations of the mean particle size.

The PSD is studied for a better understanding of the surface micromorphology, which in addition to the roughness determines the periodicity and orientation of certain motifs. The spectral display is obtained by Fast Fourier Transform (FFT). According to Fig. 4 the dominant wavelength was found at 0.554 µm for all samples with the following amplitudes: (S1) 0.879 nm, (S2) 0.691 nm, (S3) 1.17 nm, (S4) 2.67 nm, (S5) 0.501 nm and (S6) 0.441 nm.

In Fig. 5 the height and slope distribution functions are shown as normalized histograms for samples of Fig. 3 (where *p* is the corresponding quantity, height or slope; and abscissa is the tangent of the angle), computed as non-cumulative (i.e. densities). It is observed a maximum value of corresponding quantity (ρ) for sample S5.

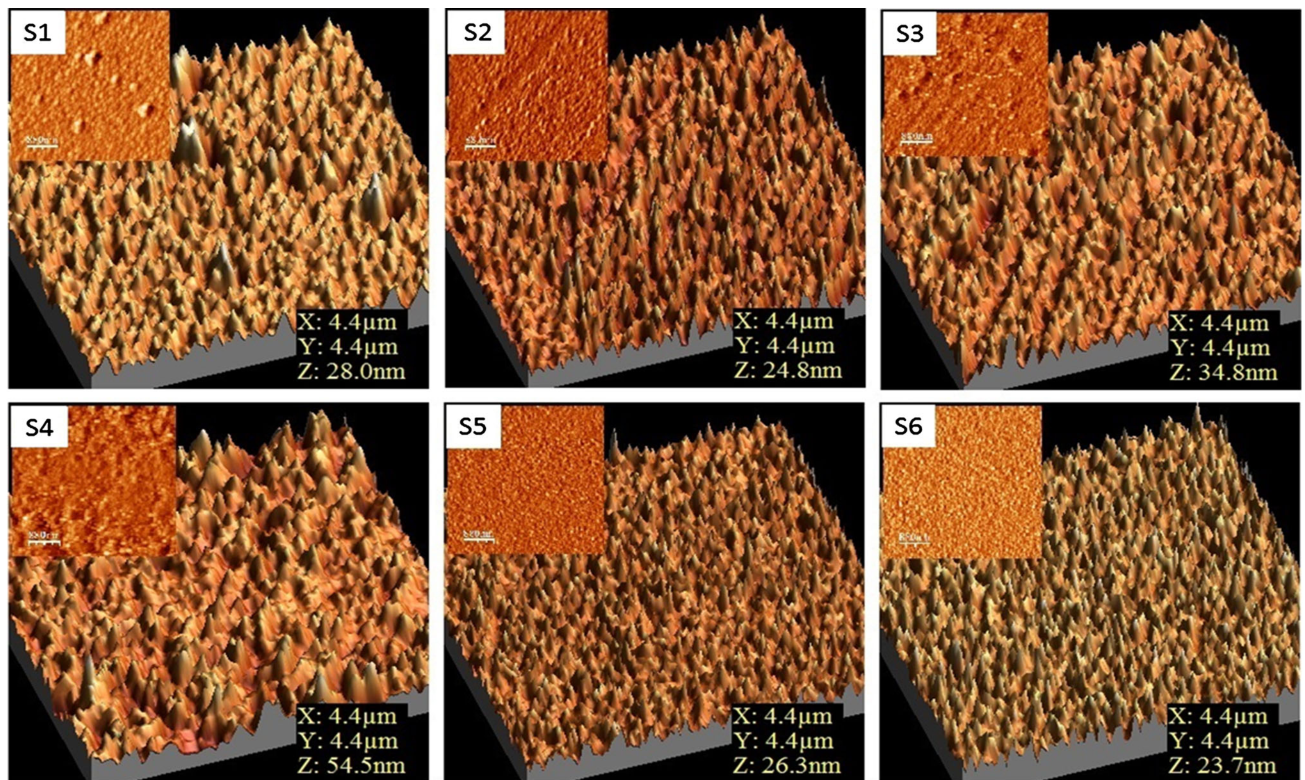

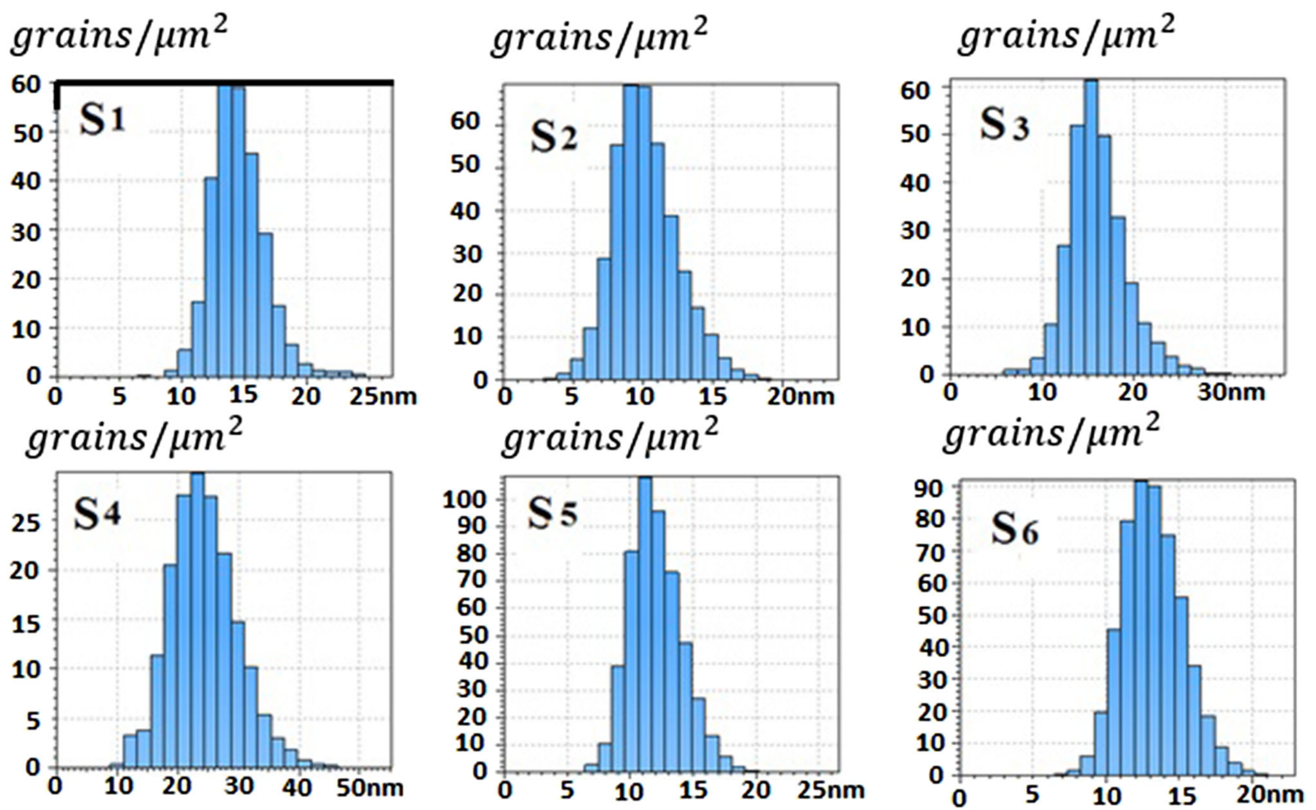

Fig. 3 Representative AFM images of samples S_i (1 to 6), and their corresponding grain size distributions

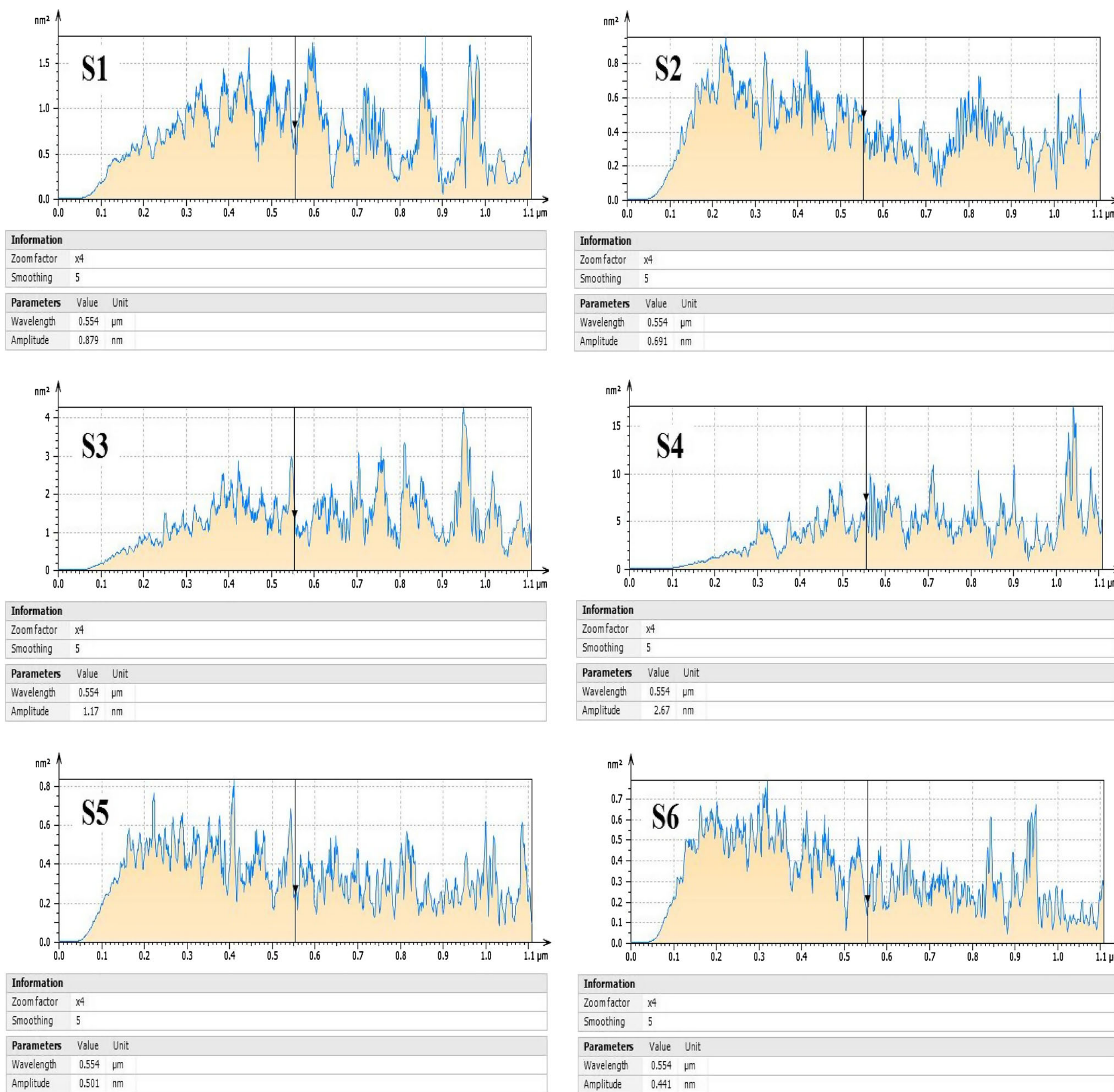

Fig. 4 The averaged power spectral density (surface) of samples S_i (1 to 6), calculated for scanning square areas of 4.4 µm × 4.4 µm

Band gap estimation in Nanostructure semiconductor thin films is to some extent difficult because the edges of the tail states due to surface atoms complicate the definition of the accurate optical band gap, thickness measuring of the nanostructure thin films is somewhat time-consuming and thicknesses aren't uniform.

The absorption spectra of as-deposited TiN thin films with different deposition temperatures are shown in Fig. 6. As it is seen, the absorption spectra revealed a red shift with increasing deposition temperature. Based on the fact that a smaller nanoparticle size will result in an absorption edge at smaller wavelengths, the observed red shifts are probably due to an increase in the grain size of the film, in agreement with the increment of the crystal size found in Fig. 2.

To determine the direct band gap of the six titanium nitride thin films, plots of $(Ah\nu)^2$ versus hν were carried out for the six titanium nitride thin films (Fig. 7). In these figure, the samples show a 'red shift' of 0.63 eV in their optical band gaps from 4.06 to 3.43 eV as the deposition temperature increases (see Table 2).We attributed this dependence to quantum confinement

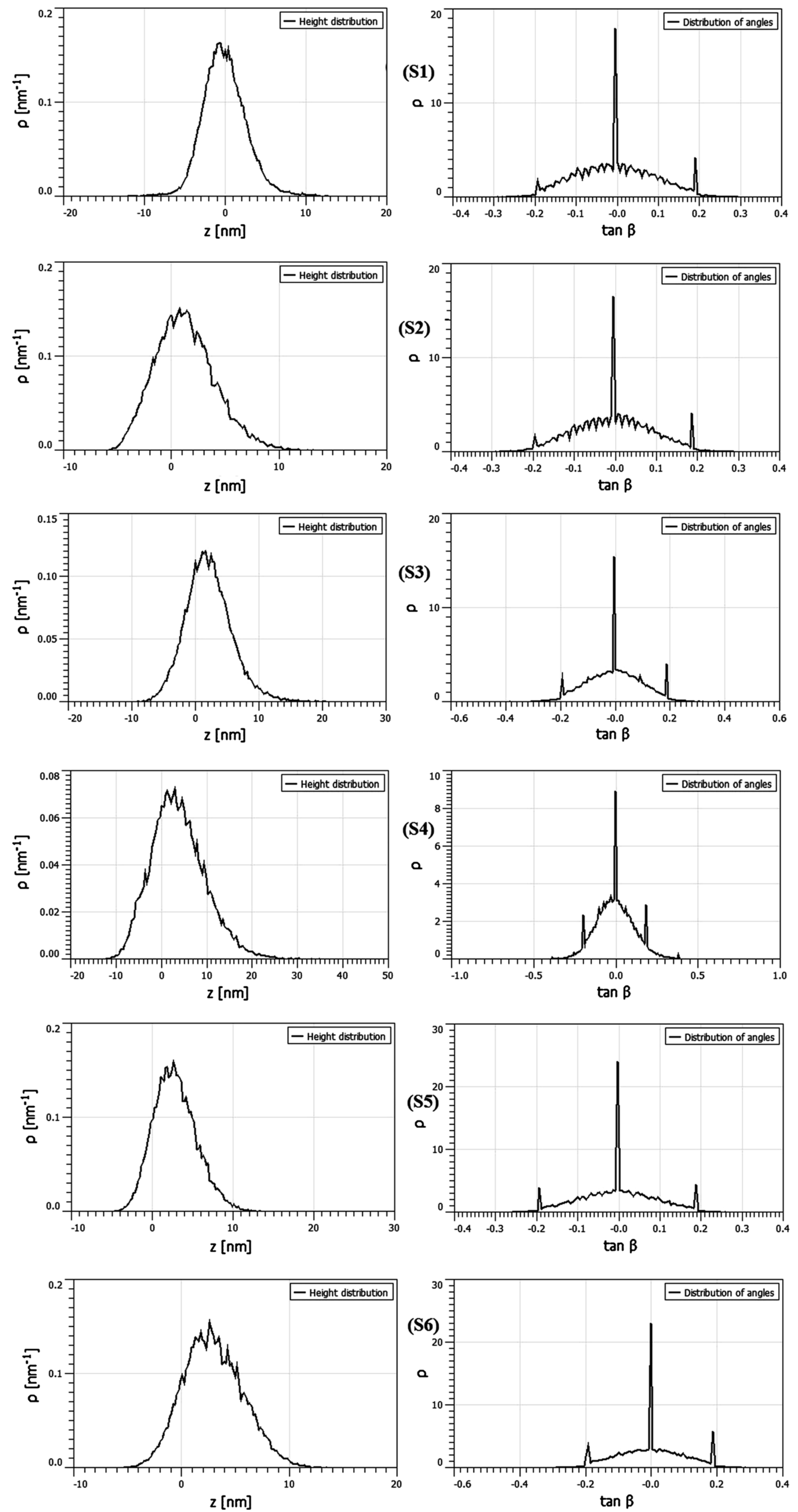

Fig. 5 Height and slope distribution functions obtained from Fig. 3

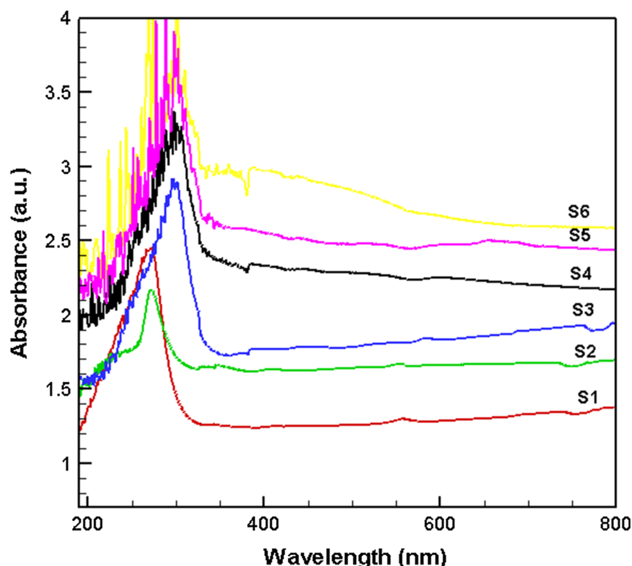

Fig. 6 UV-visible spectra of the six samples

effects that should be more important as the average grain size of the thin films decreases with the variation of the substrate temperature from 400 °C to room temperature. Moreover, surface effects could also have an important contribution in this dependence. In this regard, stoichiometric deviations are expected at the grain surface due to its reduced coordination number and roughness, which should have a notorious effect on the semiconductor properties of the thin films when the grains are in the nanoscale.

Table 2 Deposition rates, thicknesses, band-gap energies and transition index of the prepared films

No	Thickness (nm)	Deposition rate (nm/min)	Substrate temperature (°C)	Optical bandgap (eV)
S-1	565	4.7	Room temperature	4.06
S-2	405	3.4	100	3.68
S-3	650	5.4	200	3.61
S-4	650	5.4	250	3.48
S-5	650	5.4	300	3.43
S-6	485	4	400	3.43

5 Conclusions

In this work the effects of substrate temperature on the 3-D surface morphology and the optical and semiconductor properties of titanium nitride (TiN) thin films, fabricated by DC reactive magnetron sputtering, have been analyzed. Concretely, the 3-D morphology of TiN thin films grown on glass substrates was investigated at six different deposition temperatures (room temperature, 100, 200, 250, 300 and 400 °C) in order to determine the relation among the 3-D micro-textured surfaces and the optical and semiconductor properties of the samples with the substrate temperature. AFM images showed that the surface topography of the TiN nanostructured thin films changes at different deposition temperature, finding that the average grain size, the root-mean-square deviation, the skewness of

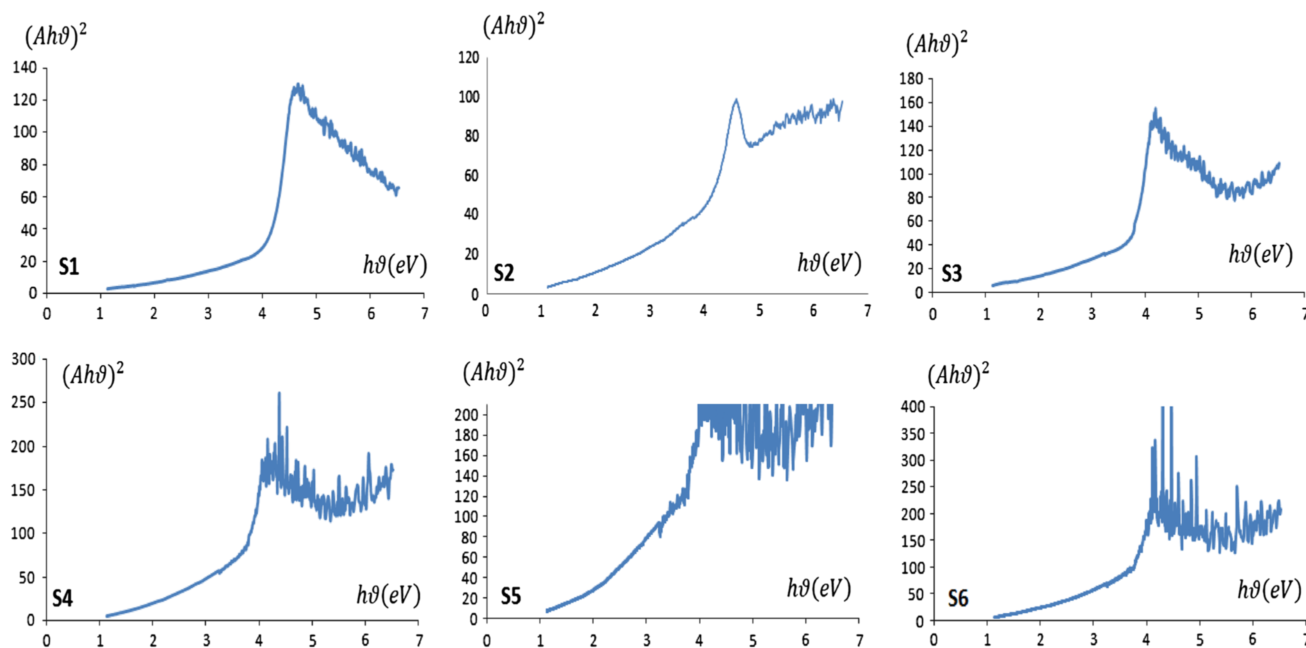

Fig. 7 Plot of $(Ahv)^2$ versus (hv) for samples with different deposition temperatures

Table 3 Root-mean-square deviation (S_q), Skewness of topography height distribution (S_{sk}), Kurtosis of topography height distribution (S_{ku}) and inclinaton angles determined from the AFM images

The basic properties of the height values distribution of the surface samples	S1 values	S2 values	S3 values	S4 values	S5 values	S6 values
Ra (Sa) (nm)	2.12	2.23	2.88	4.78	2.13	2.24
Rms (Sq) (nm)	2.78	2.81	3.74	6.09	2.68	2.78
Skew (Ssk) (−)	0.371	0.474	0.61	0.6	0.419	0.247
Kurtosis (Sku) (−)	1.59	0.373	1.39	0.858	0.339	0.0532
Inclination θ (°)	0	0	0	0	0	0
Inclination φ (°)	−94.6	25.6	100.9	37.2	91.4	163.9

topography height distribution and the kurtosis exhibit a maximum around 250 °C. Also, a competitive growth of crystalline planes with different orientations was found as a result of the occurrence of higher grain sizes in the nanostructured titanium nitride thin films. In addition, the optical band gap energy decreased from 4.06 to 3.43 eV as the substrate temperature increases from room temperature to 400 °C, due to the increment of the grain size and the subsequent reduction of quantum confinement and surface effects.

Appendix

The basic properties of the height values distribution, including its variance, skewness, kurtosis and PSD were computed according to Ref. [22]. Root-mean-square deviation (S_q), skewness of topography height distribution (S_{sk}), kurtosis of topography height distribution (S_{ku}) are parameters that depend on the height deviation, and they are useful for description of amplitude-related properties of a surface. These parameters are applied to describe dispersion, asymmetry of the height distribution and sharpness of the height distribution.

S_q, is a dispersion parameter defined as the root mean square value of the surface departures within the sampling area and is a very general and widely used parameter.

S_{sk} is the measurement of asymmetry of surface deviations about the mean reference plane and can effectively be used to describe the shape of the topography height distribution.

S_{Ku}, is a measure of the peakedness or sharpness of the surface height distribution and characterizes the spread of the height distribution.

References

1. G.L. Zhao, T.B. Zhang, T. Zhang, J.X. Wang, G.H. Han, J. Non-Cryst. Solids **354**, 1272–1275 (2008)
2. G.V. Naik, J.L. Schroeder, X. Ni, A.V. Kildishev, T.D. Sands, A. Boltasseva, Opt. Express **2**, 478–489 (2012)
3. E. Zalnezhad, A.A.D. Sarhan, M. Hamdi, Int. J. Adv. Manuf. Technol. **64**, 281–290 (2013)
4. Y. Matsumura, T. Chujo, H. Uchida, H.H. Uchida, Surf. Coat. Technol. **60**, 489–492 (1993)
5. D. Starosvetsky, I. Gotman, Biomaterials **22**, 1853 (2001)
6. S.H. Ahn, J.G. Kim, J.G. Han, Thin Solid Films **515**, 6878 (2007)
7. S.G. Wang, X.D. Bai, B.C. Wang, Y.D. Fan, Thin Solid Films **278**, 67 (1996)
8. P. Chen, W.Y. Wu, Surf. Coat. Technol. **231**, 140–143 (2013)
9. M. Molamohammadi, A. Arman, A. Achour et al., J. Mater. Sci. Mater. Electron. **26**(8), 5964–5969 (2015)
10. M. Molamohammadi, C. Luna, A. Arman et al., J. Mater. Sci. Mater. Electron. **26**(9), 6814–6818 (2015)
11. T. Ghodselahi, A. Arman, J. Mater. Sci. Mater. Electron. **26**(6), 4193–4197 (2015)
12. Ş. Ţălu, S. Stach, V. Sueiras, N.M. Ziebarth, Ann. Biomed. Eng. **43**(4), 906–916 (2015)
13. S. Kulesza, M. Bramowicz, Appl. Surf. Sci. **293**, 196–201 (2014)
14. A. Arman, T. Ghodselahi, M. Molamohammadi et al., Prot. Met. Phys. Chem. Surf. **51**(4), 575–578 (2015)
15. D. Elenkova, J. Zaharieva, M. Getsova, I. Manolov, M. Milanova, S. Stach, Ş. Ţălu, Int. J. Polym Anal. Charact. **20**(1), 42–56 (2015)
16. J.E. Sundgren, Thin Solid Films **128**, 21 (1985)
17. V. Chawla, R. Jayaganthan, R. Chandra, Mater. Charact. **59**, 1015–1020 (2008)
18. J. Ferre-Borrull, A. Duparre, E. Quesnel, Appl. Opt. **40**(13), 2190–2199 (2001)
19. A. Arman, S. Talu, C. Luna, J. Mater. Sci. Mater. Electron. (2015). doi:10.1007/s10854-015-3628-5
20. J. Tauc, A. Menth, J. Non-Cryst. Solids **569**, 8–10 (1972)
21. A. Gelali, A. Ahmadpourian, R. Bavadi, M.R. Hantehzadeh, A. Ahmadpourian, J. Fusion Energy **31**(6), 586–590 (2012)
22. Gwyddion 2.37 software (Copyright © 2004–2007, 2009–2014 Petr Klapetek, David Nečas, Christopher Anderson). Available from: http://gwyddion.net. Accessed 27 May 2015